

Supplementary methods for “Observation of nuclear fusion driven by a pyroelectric crystal”

In organic liquid scintillator (e.g., BC-501A and NE213), ionizing particles produce light pulses classified by pulse shape discrimination¹ (PSD) as either proton-like or electron-like. A proton-like pulse has relatively more long-lived scintillation components than an electron-like pulse, giving it an exaggerated tail. The vast majority of our cosmic background, due to muons and gammas, is electron-like. Neutrons, detected indirectly through proton recoil, are proton-like.

In this supplement, we discuss our neutron detection methods (B. N., S. P., and R. Cousins, in preparation). First, we calibrate the detector’s electron light output function using the Compton edges of several gamma sources. Next, we demonstrate our PSD algorithm on both an AmBe neutron source and the cosmic background. Then, we calculate, by Monte Carlo simulation, the detector’s response to 2.45 MeV neutrons. Finally, we measure our detector’s response to two neutron sources of known spectra and compare the proton recoil spectra against simulated spectra.

Electron light output calibration

Using gamma calibration sources, we establish the correspondence² between electron energy and net light output (i.e., photomultiplier anode charge). Since the relationship is found to be approximately linear and homogeneous, it will be convenient to always express light output in units of equivalent electron energy (keVee).

Simulating photon transport with the GEANT4 detector simulation toolkit³, we calculate the electron recoil spectra for monochromatic gammas incident on our detector (see Figure 1). In the scintillator, Compton scattering is the dominant interaction from about 20 keV up to and beyond our maximum gamma energy of 1.275 MeV. Below 20 keV, the photoelectric effect is the dominant means of transferring energy to electrons. Assuming single scatters in the detector, the electron recoil spectrum cuts off at the Compton edge. On the other hand, for a finite scintillator, gammas backscattered in the scintillator may continue to scatter electrons, accounting for counts above the Compton edge. Additionally, gammas backscattered from other parts of the detector contribute counts in the lower part of the spectrum, including the small peak at around 80 keV.

A single channel's calibration is shown in Figure 2. We use the simulated electron recoil spectra to locate the gamma sources' Compton edges. After convolving with a gaussian resolution function, offsetting, and scaling, the simulated spectra closely match the experimental spectra in the vicinity of the Compton edges. The resulting electron light output function is found to be nearly linear and homogeneous, as was asserted *a priori*.

Pulse shape discrimination

Typical proton-like and electron-like waveforms are shown in Figure 3. They, along with all neutron detector hits, were captured with an 8-bit 1 GS/s digitizer and stored to disk. To correct for drifting voltages, the 50 ns baseline is averaged and taken to be $V=0$. The time origin of the pulse is calculated by fitting a line to the pulse's leading edge and extrapolated back to $V=0$.

In the first step of our PSD algorithm, we make a PSD scatter plot, as shown in Figure 4. Hits enclosed within the upper region are neutron candidates. On the range [300, 1050] keV, 5% of true neutron events lie above or below this region. So, we call 95% the PSD acceptance efficiency.

In the second step of our PSD algorithm, we compare the pulse shapes of neutron candidates against tabulated proton pulse shapes. We then reject candidates that fail a χ^2 test, as shown in Figure 5. This method eliminates false neutron sources such as double gammas and PMT double pulsing. Furthermore, we monitor the 50 ns baseline to insure the RMS digitizer noise remains constant throughout the run.

We estimate the cosmic background during the run by sampling the first 100 seconds, well before neutron emission begins. As expected the PSD scatter plot resembles Figure 4b. During this interval, the average net detection rate of proton recoils was only 0.3 s^{-1} , compared with the rate of triggers recorded to disk, 900 s^{-1} .

Detector efficiency and 2.45 MeV neutron response

Using GEANT4, we simulated neutron transport through the detector and surrounding apparatus (see Figure 6). A point is randomly selected on the deuterated target as the neutron's starting point. Assuming a beam energy of 100 keV, the neutron is emitted, in the DD center-of-mass frame, at 2.45 MeV into 4π . We convert the energies of protons recoiled within the liquid scintillator into keVee using a standard proton light output table⁴.

We show the result of simulating 10^6 neutron tracks in Figure 7. The neutron response function integrated on the range [300, 1050] keVee yields a theoretical detector efficiency of 19%. Including corrections for 96% digitizer live time and 95% PSD acceptance efficiency, we arrive at the quoted net detection efficiency of 18%.

A simple calculation verifies that the tail of the Monte Carlo neutron response should be located near 950 keVee. Again assuming a beam energy of 100 keV, the lab distribution of neutron energies lies flat over $(2.45 \pm 0.33) \text{ MeV}$. Since the neutron and proton scatter elastically and have nearly equal mass, we may consider a neutron of maximum lab energy 2.78 MeV

transferring all of its energy to a proton in a single collision. Indeed, according to the proton light output function, the net light output of a 2.78 MeV proton is 950 keVee.

Comparison against known spectra

To confirm our neutron detection methods, we have measured our detector's response to both AmBe and ^{252}Cf neutron sources. These proton recoil spectra, including fits to simulated spectra, are shown in Figure 8.

1. Brooks, F. D. A scintillation counter with neutron and gamma-ray discriminators. *Nucl. Instr. and Meth.* **4**, 151–163 (1959).
2. Dietze, G. & Klein, H. Gamma-calibration of NE 213 scintillation counters. *Nucl. Instr. and Meth.* **193**, 549–556 (1982).
3. Agostinelli, S. *et al.* GEANT4—a simulation toolkit. *Nucl. Instr. and Meth. A* **506**, 250–303 (2003).
4. Verbinski, V. V. *et al.* Calibration of an organic scintillator for neutron spectrometry. *Nucl. Instr. and Meth.* **65**, 8–25 (1968).
5. Marsh, J. W., Thomas, D. J. & Burke, M. High resolution measurements of neutron energy spectra from Am-Be and Am-B neutron sources. *Nucl. Instr. and Meth. A* **366**, 340–348 (1995).
6. Lajtai, A., Dyachenko, P. P., Kononov, V. N. & Seregina, E. A. Low-energy neutron spectrometer and its application for ^{252}Cf neutron spectrum measurements. *Nucl. Instr. and Meth. A* **293**, 555–561 (1990).

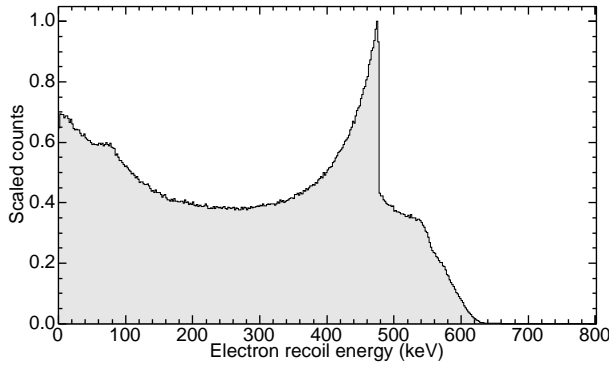


Figure 1: Our detector's Monte Carlo electron recoil spectrum for 662 keV ^{137}Cs gammas. Shown histogrammed is the net energy transferred to scattered electrons, including possible multiple scatters, per simulated incident gamma. The Compton edge is at 478 keV.

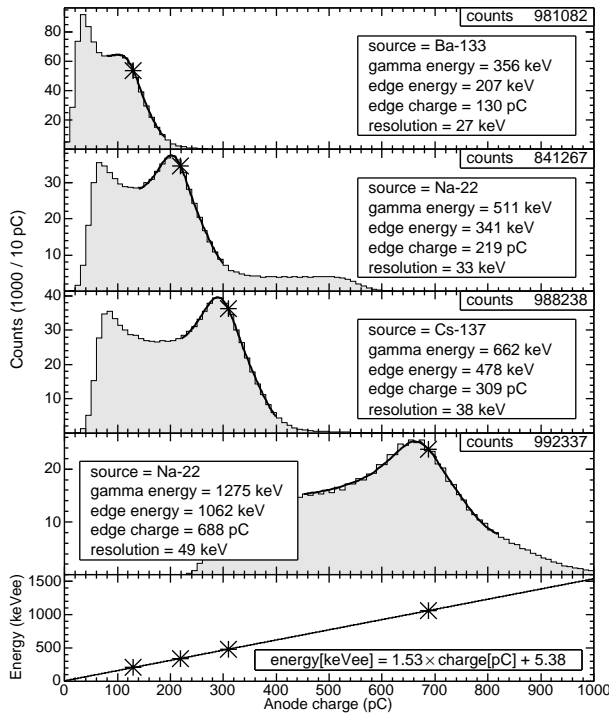


Figure 2: A single channel's four point electron response calibration. We precisely locate the Compton edges by fitting to simulated responses, shown by the smooth curves. This particular calibration was made *in situ* immediately prior to the run presented in Figure 2 of the Letter. Similar calibrations were made for the other five neutron detector channels.

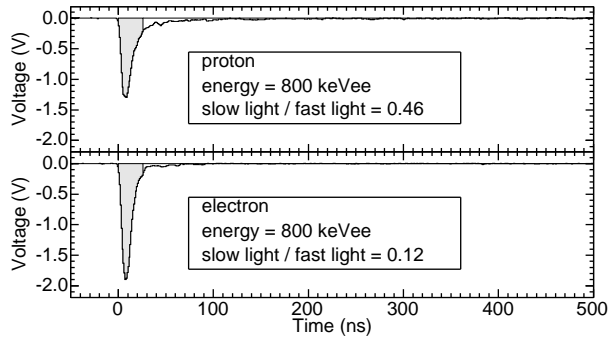


Figure 3: Typical proton-like and electron-like waveforms. Both have the same electron equivalent energy 800 keVee. Our PSD variable (“slow light / fast light”) is the ratio of integrated tail light to integrated peak light (shown shaded). At 800 keVee, the dividing point between peak and tail is 26 ns. More generally, the dividing point is a function of pulse energy chosen to maximize a figure of merit.

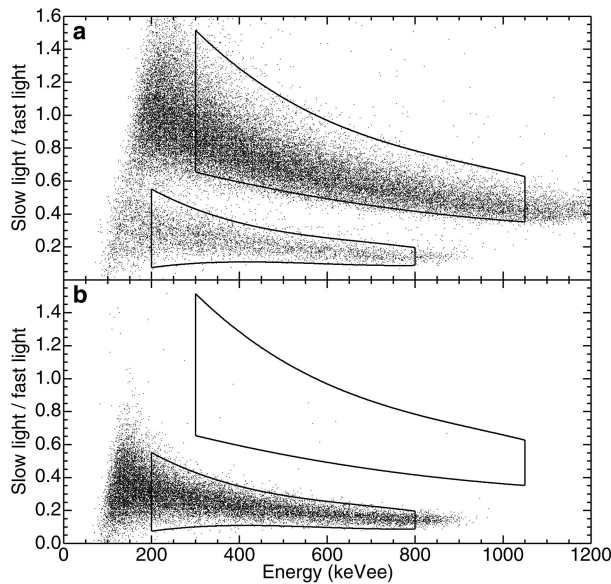


Figure 4: Demonstration of PSD algorithm. **a**, AmBe neutron source. The upper branch is due to neutrons scattering protons within the liquid scintillator, while the lower branch is due to AmBe’s 4.4 MeV gammas scattering electrons within the liquid scintillator. Triggering on the coincidence of a second scintillator separated by a 10 cm lead shield, neutrons were preferentially collected. **b**, Cosmic background. Note the cosmic background is predominantly electron-like.

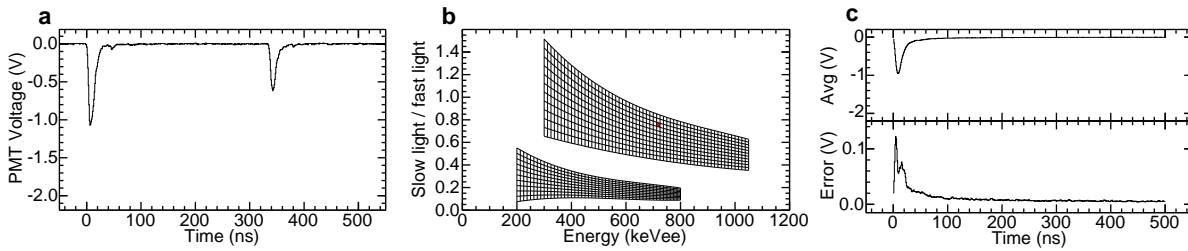


Figure 5: Rejection of a neutron candidate. **a**, This event, occurring at $t = 140$ s during the run, shows a gamma pile-up event whose ratio of slow light to fast light placed it in the proton region. **b**, For comparison, we have a catalog of typical waveforms and their associated errors of measurement, indexed according to the cells shown. Our candidate event lies in the cell shaded red. **c**, Comparing the candidate event against the typical waveform using the reduced χ^2 as a metric, the candidate neutron was rejected.

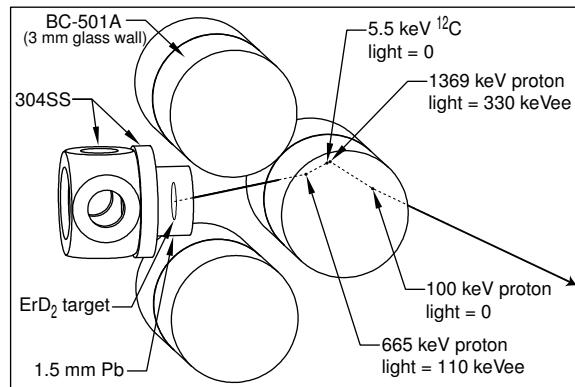


Figure 6: Sample Monte Carlo neutron track. In this case, the neutron's initial energy in the lab frame was 2.74 MeV. The neutron scattered three protons in a single liquid scintillator cell, giving a net light output of 440 keVee.

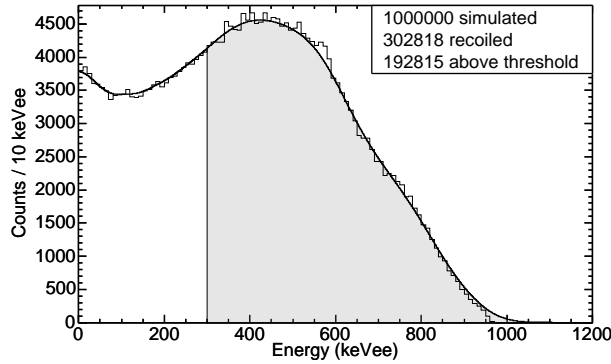


Figure 7: Monte Carlo 2.45 MeV neutron response. Out of 10^6 simulated neutron tracks, 30% scattered protons in the detector. The net light output per track is shown histogrammed. We convolute this histogram with the detector's resolution function to obtain the 2.45 MeV neutron response function, indicated by the smooth curve. In Figure 3b of the Letter, this calculated response function matches the experimental neutron spectrum.

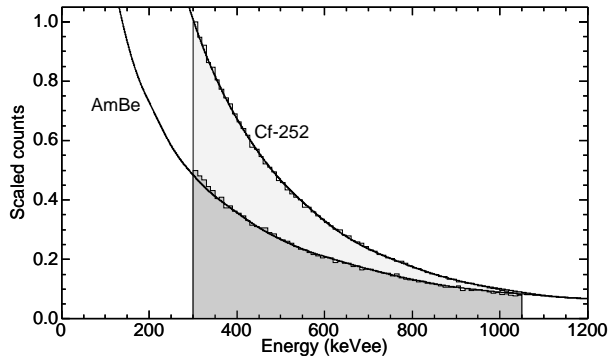


Figure 8: Proton recoil spectra of AmBe and ^{252}Cf . The histograms are our experimental spectra, while the smooth curves are the simulated spectra derived from the sources' known neutron spectra^{5, 6}. The AmBe source was behind 10 cm of lead, and the ^{252}Cf source was behind 5 cm of lead. The techniques used to measure and simulate the proton recoil spectra are identical to those used in Figure 3 of the Letter.